ISSN 1070-3284, Russian Journal of Coordination Chemistry, 2023, Vol. 49, No. 9, pp. 542–554. © Pleiades Publishing, Ltd., 2023.
Russian Text © The Author(s), 2023, published in Koordinatsionnaya Khimiya, 2023, Vol. 49, No. 9, pp. 530–542.

Synthesis, Structure, and Properties of the Iron Nitrosyl Complex with 2-Ethyl-4-pyridinecarbothioamide

N. A. Sanina[a, b, c, *], G. V. Shilov[a], N. S. Ovanesyan[a], V. A. Mumyatova[a], A. A. Balakina[a], A. A. Terent'ev[a, b, c], O. V. Pokidova[a], and S. M. Aldoshin[a]

[a] *Federal Research Center of Problems of Chemical Physics and Medicinal Chemistry, Russian Academy of Sciences, Chernogolovka, Russia*

[b] *Research and Education Center "Medicinal Chemistry" in Chernogolovka, State University of Education, Mytishchi, Moscow oblast, Russia*

[c] *Moscow State University, Moscow, Russia*

**e-mail: sanina@icp.ac.ru*

Received February 28, 2023; revised March 17, 2023; accepted March 22, 2023

Abstract—The synthesis and data on the physicochemical characteristics and biological activity of the new iron nitrosyl complex $(Q^+)_2[Fe_2(S_2O_3)_2(NO)_4]^{2-}$ (**I**), where Q^+ is protonated 2-ethyl-4-pyridinecarbothioamide ($C_8H_{11}N_2S$), are presented. The structure and properties of the complex were studied by X-ray diffraction, elemental analysis, IR and Mössbauer spectroscopy, and amperometry. The complex showed antibacterial activity and efficiently inhibited cyclic guanosine monophosphate phosphodiesterase (cGMP PDE), which may suggest its antihypertensive, anti-aggregation, and vasodilator activities.

Keywords: binuclear iron(I) tetranitrosyl complexes, X-ray diffraction, IR spectroscopy, Mössbauer spectroscopy, amperometry, antibacterial activity, biofilms, ampicillin, kanamycin, streptomycin, ceftriaxone, MTT assay, phosphodiesterase

DOI: 10.1134/S1070328423600523

INTRODUCTION

Endogenous nitric oxide (NO) plays an important role as a first-line defense against various pathogens: it efficiently acts on viruses [1, 2] and possesses antibacterial and antifungal [3–5] activities. The formation of NO is enhanced in macrophages induced by infectious agents or cytokines [6].

The exogenous agents for NO generation considered as antimicrobial agents can be divided into several main classes [7]. Apart from NO gas and various NO generation systems [8–16], it is possible to use organic nitrates [17], NONO-ates [18, 19], and S-nitrosothiols [20–22]. In recent years, there has been increased interest in low-molecular-weight mimetics of nitrosyl ferredoxins containing a natural $Fe(NO)_2$ group [23, 24]. The following mechanisms of the antimicrobial action of NO donors of this class are considered: (1) induction of oxidative and nitrosative stress [9]; (2) modification of thiol-containing amino acids in proteins [25]; (3) nitrosylation and transcription factor NF-κB dysfunction [26]. In view of the similarity of the structures of iron nitrosyl complexes (INCs) and natural nitrosyl proteins [1Fe–2S] and [2Fe–2S], it is expected that their antimicrobial action would involve new mechanisms not related to DNA as the primary target. These mechanisms require additional research including the synthesis of new INCs, most often containing ligands that possess antimicrobial activity, and their investigation using in vitro and in vivo models.

In the vast majority of cases, aliphatic and aromatic thiols are used as ligands for the synthesis of INCs [27–30]. Iron nitrosyl complexes based on thioamides are virtually unknown, but are of high practical interest. Thioamide derivatives show antituberculosis [31, 32], antiviral [33], anticancer [34, 35] and fungicidal [36] activities and anthelminthic and thyrotoxic effects [37]. Thioamides have higher antibacterial and antiviral activities than the corresponding amides [38–43]. 5-Acetoxy- and 5-hydroxyalkanethioamide analogues showed a high antibacterial activity against *Staphylococcus aureus* [44]. There are pharmaceutical compounds containing thiocarbonyl groups, including methylthiouracil and propylthiouracil, antithyroid drugs that decrease the synthesis of thyroxine in the thyroid gland and thus have a therapeutic action against hyperthyroidism; antituberculosis drug thiacetazone; enzalutamide acting as an androgen receptor agonist; antimetabolite thioguanine, etc. [45]. As natural thioamides are being found, synthetic strategies towards the development of therapeutic agents containing peptide thioamides are developed [46].

A number of aromatic thioamide derivatives are used as efficient drugs for the treatment of tuberculosis. Among them are ethionamide and isoniazid. The structures of ethionamide (A) and isoniazid (B) are depicted in Scheme 1.

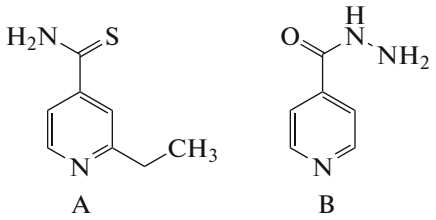

Scheme 1.

The mechanism of their action is related to suppression of the protein synthesis in mycobacteria. Ethionamide inhibits the growth and reproduction of tuberculosis mycobacterium with both intracellular and extracellular positions (in particular, it acts on the refractory and atypical forms); enhances phagocytosis in the focus of tuberculous inflammation; and is used in combination with other agents in those cases where the first-line drugs are ineffective or contraindicated. The effective bacteriostatic action of ethionamide against isoniazid-resistant strains was demonstrated in experiments and clinical trials on animals [47]. The ethionamide activity is pH-dependent: it increases in acidic media [48]. Despite the fact that ethionamide and its structural analogues are widely used in therapy and that data on their crystal structures are available from the literature [49], there is still little information on their important physicochemical characteristics such as solubility, separation in pharmaceutically important solvents, and membrane permeability [50, 51].

In this connection, hybrid systems containing two important pharmacophores, NO group and thioamide, as ligands may be promising in the NO therapy of infectious diseases. Our data [52] indicate that compounds containing the $\{Fe(NO)_2\}^9$ structural moiety and a thioamide as parts of an NO-releasing hybrid molecule may exhibit synergism of anti-infective, anti-inflammatory, and immunomodulatory properties.

The purpose of this study is to prepare the iron nitrosyl complex $(C_8H_{11}N_2S^+)_2[Fe_2(S_2O_3)_2(NO)_4]^{2-}$ (**I**) and to investigate its structure and properties in the solid state and in solutions and the biological activity.

EXPERIMENTAL

Iron nitrosyl complex **I** was prepared by a low-temperature synthesis using commercial chemicals, which were used as received: NaOH (Aldrich), $Na_2S_2O_3\cdot 5H_2O$ (Aldrich), HCl (reagent grade, 37%), and 2-ethyl-4-pyridinecarbothioamide (Aldrich). The synthesis of INC **I** included three stages: (1) preparation of gaseous NO by known procedure [53]; (2) synthesis of INC precursor with the thiosulfate ligand $Na_2[Fe_2(S_2O_3)_2(NO)_4]\cdot 2H_2O$ according to reported procedure [54]; and (3) synthesis of INC **I** with 2-ethyl-4-pyridinecarbothioamide (see Scheme 1). All operations on the preparation, mixing, and storage of solutions were performed in an argon atmosphere. Solutions were prepared using doubly distilled water. The solvents, methanol and dimethyl sulfoxide (DMSO), were purified by known procedures [55].

Synthesis of I. A dry mixture of $Na_2[Fe_2(S_2O_3)_2(NO)_4]\cdot 2H_2O$ (0.77 mM) and $Na_2S_2O_3\cdot 5H_2O$ (0.4 mM) was dissolved in water (5 mL), and the solution was filtered into a reaction flask. A weighed portion (3.5 mM) of 2-ethyl-4-pyridinecarbothioamide (Scheme 1) was dissolved in concentrated HCl (1 mL) and water (3 mL), and the solution was filtered into the reaction flask with intense magnetic stirring at room temperature. The dense and thick light brown amorphous precipitate that formed instantaneously was stirred for 20 min, then collected on a membrane filter, and dried in an argon flow at room temperature. The yield of **I** was 85%.

For $C_{16}H_{22}N_8O_{10}S_6Fe_2$ (**I**)						
Anal. calcd., %	C, 24.31	H, 2.81	N, 14.17	O, 20.24	S, 24.34	Fe, 14.13
Found, %	C, 24.30	H, 2.84	N, 14.20	O, 20.22	S, 24.33	Fe, 14.11

The single crystals of **I** for X-ray diffraction were obtained by recrystallization of the amorphous precipitate from methanol by slow (for 2 weeks) removal of the solvent at −18°C.

Elemental analysis for C,H,N,S,O was performed on a Vario El cube CHNS/O elemental analyzer at the Analytical Center for Collective Use at the Federal Research Center of Problems of Chemical Physics and Medicinal Chemistry, Russian Academy of Sciences. Iron was quantified by atomic absorption spectrophotometry on an AAS-3 ainstrument (Carl Ceiss Jena, Germany) in an acetylene–air flame using a deuterium background corrector. A lamp with a hollow cathode was used. Iron determination was based on the resonance line $\lambda = 248.3$ nm.

The IR spectrum of **I** was measured on a Bruker ALPHA FTIR spectrometer in the frequency range of 400–4000 cm^{-1} in the attenuated total reflectance (ATR) mode.

IR (ν, cm^{-1}): 3284 w, 3132 w, 2697 vw, 1780 m, 1758 vs, 1650 w, 1632 w, 1425 vw, 1362 vw, 1290 vw, 1255 w, 1231 w, 1188 m, 1141 vw, 1016 m, 924 vw, 838 w, 815 vw, 775 vw, 735 vw, 710 vw, 686 vw, 600 m, 530 m.

X-ray diffraction of I was carried out on an XCalibur diffractometer with an EOS CCD detector (Agilent Technologies UK Ltd, Yarnton, Oxfordshire, England). The collection of reflections and unit cell parameter determination and refinement were carried out at 100 K using monochromatized MoK_α radiation with $\lambda = 0.71073$Å and the CrysAlis PRO software

Table 1. Main crystallographic data and X-ray experiment and structure refinement details for **I**

Parameters	Value
Molecular formula	$C_{16}H_{22}N_8O_{10}S_6Fe_2$
M	790.47
Temperature, K	100(1)
Crystal size, mm	0.15 × 0.10 × 0.05
λ, Å	0.7107
System	Triclinic
Space group	$P\bar{1}$
a, Å	7.3417(4)
b, Å	7.4792(4)
c, Å	14.0322(11)
α, deg	78.174(5)
β, deg	82.408(5)
γ, deg	78.372(5)
V, Å^3	735.35(8)
Z	1
ρ(calcd.), g/cm^3	1.785
μ, mm^{-1}	1.476
F(000)	402
Measurement range on θ, deg	26.069
Measured reflections (R_{int})	5513
Unique reflections	2907
GOOF	1.247
R_1, wR_2 ($I > 2\sigma(I)$)	0.0829, 0.2067
R_1, wR_2 (all data)	0.0862, 0.2081
Residual electron density (max/min), e Å^{-3}	1.857/–0.806

[56]. The structure was solved by direct methods. The positions and thermal parameters of non-hydrogen atoms were refined anisotropically by the least-squares method. All calculations were performed with the SHELXTL program package [57]. The hydrogen atom positions in the anion were revealed from the difference maps and refined in the riding model. The positions of hydrogen atoms of the water molecule were derived from the Fourier difference maps and refined with constraints imposed on the bond lengths and thermal parameters. The unit cell parameters and the main crystallographic data for **I** are summarized in Table 1.

The full set of X-ray diffraction data was deposited with the Cambridge Crystallographic Data Centre (CCDC no. 2243554; www.ccdc.cam.ac.uk/data_request/cif).

The Mössbauer absorption spectra of a polycrystalline powder of **I** were recorded on a WissEl unit (Wissenschaftliche Elektronik GmbH, Germany) operating in the constant voltage mode. The Co^{57} isotope in Rh matrix at room temperature served as the radiation source. The Mössbauer spectra were processed by the least-squares method with the assumption of the Lorentzian shape of the composite absorption lines.

Measurement of the NO donor activity. The NO donor activity of **I** in solutions was determined using an amiNO-700 sensor electrode (inNO Nitric Oxide Measuring System, Innovative Instruments, USA). The method is based on the measurement of the diffusion current resulting from a change in the electrode potential upon the release of NO by the test compound. The concentration of NO generated by INC **I** over 500 s was measured with a 0.2 s step in a 0.1% aqueous solution of DMSO with the 0.4 × 10^{-5} M concentration of the complex (pH 7.0; T = 25°C). The amperometric sensor was calibrated using a standard 1 μM aqueous solution of $NaNO_2$, which was added to a mixture containing H_2O (18 mL), KI (20 mg), and reagent grade 1 M H_2SO_4 (2 mL). The reaction is described by the equation

$$2NaNO_2 + 2KI + 2H_2SO_4$$
$$= 2NO\uparrow + K_2SO_4 + 2H_2O + Na_2SO_4 + I_2,$$

according to which the compounds react in 1 : 1 : 1 ratio. This means that the concentration of the released NO is equivalent to the concentration of added nitrite. The addition of 10 μL of the standard solution of sodium nitrite results in the release of 50 nM of NO in 20 mL of the formed solution. The calculation is performed by the following relation:

$$M_1V_1 = M_2V_2,$$

where M_1 is the molar concentration of the nitrite solution; V_1 is the added volume of the standard nitrite solution; M_2 is the molar concentration of the nitrite after the standard has been added to the flask; V_2 is the total volume. After that, as portion of INC **I** was dissolved in DMSO (10 mL), a sample $V = 0.5$ mL was taken and added to 49.5 mL of Buffer Hidrion solution (Sigma-Aldrich, USA) with pH 7.0, and NO release was measured.

Antibacterial activity assay. The antibacterial activity of **I** was evaluated by determining the minimum inhibitory concentration (MIC) and the ability to inhibit the formation of bacterial biofilms. MIC was determined by the micromethod of serial dilutions according to the requirements of Methodical Guidelines MUK 4.2.1890-04 [58]. The serial dilution method is a modern, standardized, and most accurate method for gaining a quantitative characteristic of sensitivity of microorganisms to antibacterial agents. The study was carried out using the gram-negative *Escherichia coli* (BB strain) and gram-positive *Micrococcus luteus* (21/26 strain). For experiments, working suspensions of both bacterial cultures were prepared, diluted 100-fold, and seeded into the wells of 96-well plates (100 μL per well). The final concentration of the bacterial agent in a well was 5×10^5 CFU/mL. The test complex **I** and its components were dissolved in DMSO to a starting concentration of 200 mM. Immediately before deposition, compounds were diluted 100-fold with a sterile LB medium (1% peptone; 0.5% yeast extract; 1% NaCl; 0.1% glucose; pH 6.8–7.0) and introduced into the wells of 96-well plates containing the bacterial suspension (100 μL per well). The final solutions of the test compounds represented 12 serial twofold dilutions from 1000 to 0.47 μM. The final concentration of DMSO was 10% in all samples. This DMSO concentration did not affect the viability of the bacteria. The control samples were grown in the LB medium, in the LB medium with 10% DMSO at 37°C, and in the LB medium at 4°C as the negative control. After the addition of test compounds, the samples were incubated at 37°C for 24 h. The control antibacterial agents included ampicillin (OJSC Sintez, Russia), kanamycin (OJSC Sintez, Russia), streptomycin (OJSC Biokhimik, Russia), and ceftriaxone (OJSC Biokhimik, Russia). The antibiotics were dissolved in sterile LB medium. The final antibiotic concentrations were 12 serial twofold dilutions from 1000 to 0.47 μM.

After 24 h from the beginning of the incubation, the results were analyzed. MIC was found as the concentration at which no visible microbial growth was present in comparison with the control.

Study of *M. luteus* biofilm formation. For the experiment, a working bacterial suspension was seeded into a 96-well plate, and the test compound and antibiotics were added to the wells in concentrations corresponding to MIC. The control samples were grown in LB, in LB with 10% DMSO, and in LB without a bacterial agent to determine the background staining of the substrate. The plates were incubated at 37°C for 24 h. Then the medium with the plankton cells was removed, the wells were washed with the sterile PBS buffer (137 mM NaCl, 2.68 mM KCl, 4.29 mM Na_2HPO_4, 1.47 mM KH_2PO_4, pH 7.4) and dried to fix the biofilms on the substrate, and the biofilms were stained with a 0.1% solution of Gentian Violet. Then the wells were washed with water and dried at 37°C for 60 min. The dye bound to the biofilms was dissolved in 95% ethanol, and the absorbance of the resulting solutions was determined photometrically at a wavelength of 570 nm. The absorbance of the solution in the control samples containing a bacterial suspension without the test complexes was taken to be 100%. The background staining of the substrate (empty wells) was subtracted from the results for all samples.

Study of the cytotoxic properties. The work was performed on a Vero cell culture (African green monkey kidney epithelial cells) received from the collection of the Institute of Cytology, Russian Academy of Sciences. The cells were cultured using the standard procedure in 5% CO_2 atmosphere at 37°C in DMEM medium (PanEco, Russia) containing 10% fetal calf serum (BioWest, France), penicillin (50 U/mL), and streptomycin (50 mg/mL). The cytotoxic properties were determined using the MTT assay. The cells were seeded in 96-well culture plates in concentration of 5×10^4 cells/mL. The compounds were added to the culture medium 24 h after seeding. Immediately before being introduced into the culture medium, the compounds were dissolved in DMSO to a maximum concentration of 500 mM. The final DMSO concentration in the samples did not exceed 0.1%. Within 72 h after the addition of the test compounds, 3-(4,5-dimethylthiazol-2-yl)-2,5-diphenyl-2H-tetrazolium bromide (MTT, Dia-M, Russia) was added to the incubation medium in a concentration of 0.5 mg/mL. Staining was carried out for 3 h in 5% CO_2 at 37°C. The resulting formazan crystals were dissolved in 100% DMSO. The absorbance was measured at the main wavelength of 570 nm and at a background wavelength of 620 nm using a Spark 10M multifunctional plate reader (Tecan, Switzerland). The cytotoxicity index (IC_{50}) was determined on the basis of dose-dependent curves.

Study of the PDE inhibiting activity. The cyclic guanosine monophosphate phosphodiesterase (cGMP PDE) activity in the presence of complex **I** and its components was determined from the amount of guanosine monophosphate (GMP) formed in the enzymatic reaction; in turn, this amount was equivalent to the amount of inorganic phosphate generated from GMP upon the addition of 5'-nucleotidase [59] (Scheme 2):

$$\text{cGMP} \xrightarrow{\text{cGMP PDE}} \text{GMP} \xrightarrow{\text{Nucleotidase}} PO_4^{3-} + \text{guanosine}.$$

Scheme 2.

Commercial cGMP, ATP (Sigma Aldrich, USA), DMSO, trichloracetic acid (TCA), ammonium molybdate (Reakhim, Russia) after appropriate purification, and Tris-HCl buffer (Serva, Germany) were used. The cGMP PDE enzyme was isolated from the brain cortex of Wistar rats [59]. The brain tissue was homogenized in a Potter homogenizer in a 10-fold weight amount of cooled 0.2 M Tris-HCl buffer, pH 7.55. The homogenate was centrifuged for 1 h at 40000 *g*. The supernatant containing cGMP PDE was frozen in liquid nitrogen.

The effect of **I** and its components on the enzyme activity was studied and the inhibition constant was determined by the method tested previously [60], which consists in measuring the concentration of phosphates formed in the reaction (Scheme 2). For this purpose, an aliquot portion of an cGMP PDE solution containing 0.1 mg of the protein was added to 1 mL of 0.2 M Tris buffer (pH 7.6). The test compounds were added as DMSO solutions (0.2 mL), with their final concentration being 0.1, 0.01, or 0.001 mM. The total sample volume was 2.0 mL. After 15 min of preincubation at room temperature, 0.1 mM cGMP was added. The samples were incubated for 20 min at 30°C and then placed into a boiling water bath for 3 min. Then the samples were cooled to room temperature, nucleotidase (as cobra venom) (50 μg) was added, and the samples were incubated at 30°C for 10 min. The reaction was arrested by adding 55% TCA (0.2 mL) to each sample. The reaction mixture was centrifuged at 10000 *g* for 5 min. To determine the activity of cGMP PDE, the content of inorganic phosphate formed in the enzymatic reaction was measured spectroscopically upon reaction with ammonium molybdate at $\lambda = 735$ nm using a Specord M-40 spectrophotometer. The relative enzyme activity was calculated by the formula

$$I = 100(A_0 - A)/A_0,$$

where I is the relative activity; A_0 is the specific content of the inorganic phosphate in the control sample (without the test compound); A is the specific content of the inorganic phosphate in the test sample (in the presence of the test compound).

To determine the character of inhibition for **I**, the dependence of the rate of the enzymatic reaction on the substrate concentration was investigated in the presence and in the absence of the complex [61].

RESULTS AND DUSCUSSION

The starting ethionamide is insoluble in water, but is readily soluble in the acidic aqueous solutions, and is introduced in this form in the reaction at room temperature. Complex **I** is formed via exchange reaction between the sodium cation of $Na_2^+[Fe_2(S_2O_3)_2(NO)_4]^{2-}$ and the protonated ethionamide in acidic aqueous solution according to Scheme 3:

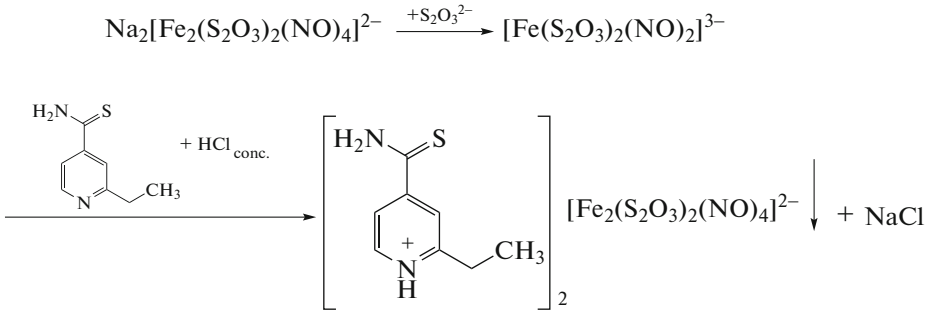

Scheme 3.

Compound **I** crystallizes in the triclinic system, and the crystal structure was refined in a centrosymmetric group. Figure **1** shows the molecular structure of **I**. The asymmetric part includes a half of the centrosymmetric binuclear nitrosyl iron with two thiosulfate ligands and the ethionamide ion. Each iron atom occurs in a tetrahedral environment formed by two nitrogen atoms of the NO ligands and two bridging S

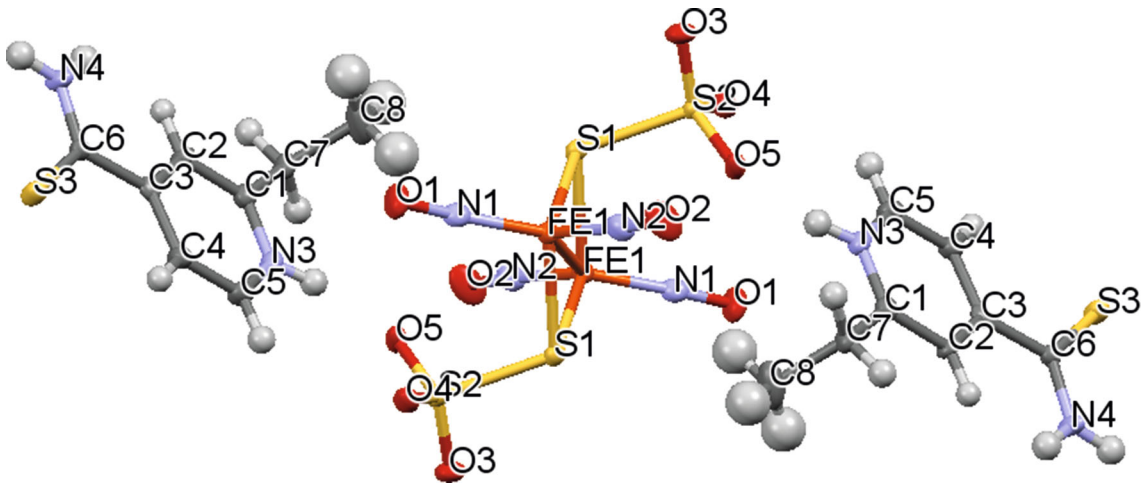

Fig. 1. Molecular structure of complex **I**.

atoms of the dithiosulfate anions. The charge of the binuclear anion is −2. Two ethionamide cations per binuclear dianion are present in the structure. It should be noted that the hydrogen atom at N(3) was found from the difference density maps rather than calculated geometrically from the electroneutrality condition. Table 2 summarizes the bond lengths and bond angles of **I**. The Fe–N and N–O bond lengths and FeNO angles in **I** coincide to within 3 sigma.

Figure 2 shows the packing of **I**. A unit cell contains one binuclear $[Fe_2(S_2O_3)_2(NO)_4]^{2-}$ dianion and two $\{C_8H_{11}N_2S\}^+$ ethionamide cations protonated at the pyridine nitrogen.

Figure 3 shows the chains of intermolecular contacts involving the NO groups of the dianion of **I**; their lengths are presented in Table 3. It can be seen that out of the two independent groups, only one N(2)–O(2) group is involved in intermolecular contacts with the bridging sulfur atoms of the dianion and the carbon atom of the cation. In all probability, this is reflected in the difference between the angles: the O(1)N(1)Fe(1) angle is 169.5(7)° and the O(2)N(2)Fe(1) angle is 172.5(8)°.

Along with the ionic contacts, hydrogen bonds exist in the crystal structure (Fig. 4) between the atoms of the complex dianion and the cation. Table 4 summarizes the hydrogen bond lengths. The crystal structure of **I** is stabilized by ionic interactions and hydrogen bonds. There are only two types of hydrogen bonds involving hydrogens of the exo- and endocyclic amino groups, N(3) and N(4), and oxygens of the sulfo groups. The characteristics of the hydrogen bonds are given in Table 4.

Thus, the interactions between the anion and the cation include electrostatic contacts and hydrogen bonds between exo- and endocyclic amino groups (N(3) and N(4)) and the sulfo-group oxygen atoms.

The Mössbauer spectral parameters for the powder of **I** (isomer shift δ_{Fe} = 0.090(3) mm/cm; quadrupole splitting ΔE_Q = 1.126(6) mm/cm, and line width Γ = 0.275(8) mm/cm at T = 293 K) were close to those of neutral iron tetranitrosyl complexes of the μ-S structural type with the $[Fe_2(S_2O_3)_2(NO)_4]^{2-}$ dianion, which we studied previously [62–64].

It was found that in 1% aerobic aqueous solutions of DMSO, compound **I** releases NO without additional activation (photo, thermal, or redox agents). The release of NO upon decomposition of the complex is already observed several seconds after dissolution. Figure 5 shows the kinetic dependences for **I**: the NO generation is more efficient in neutral aerobic solutions of **I** (18.2 nM) than in anaerobic solutions (2.8 nM). By the 250th second, the curves reach a plateau, and the amount of the released NO does not decrease by the 500th second of the experiment, indicating that long-lived nitrosyl intermediates are formed in the solution of this complex and can provide long-term NO-donor activity. Complex **I** contains the $[Fe_2(S_2O_3)_2(NO)_4]^{2-}$ dianion. Mass spectrometric analysis of a solution of a complex with the same dianion demonstrated that within ~4 min after the preparation, the mass spectrum exhibited mainly the $[Fe(S_2O_3)(NO)_2]^-$, $[Fe(S_2O_3)(NO)]^-$, and $[Fe(S_2O_3)]^-$ ions in 1 : 0.47 : 0.16 ratio. After 24 min, the content of the major $[Fe(S_2O_3)(NO)_2]^-$ ions was 40%, while 64 min later it amounted to 10% of the initial value, with the intensity ratio of this ion and the $[Fe(S_2O_3)(NO)]^-$ and $[Fe(S_2O_3)]^-$ ions being invariable [65]. Note that pH of the solution affects the amount of NO released by complex **I**, while the course of the kinetic curves does not change: in more acidic media, the NO generation increases (both in aerobic and anaerobic solutions), while in alkaline oxygen-containing solutions it decreases (Table 5).

Table 2. Selected bond lengths and bond angles for **I***

Bond	*d*, Å	Bond	*d*, Å
Fe(1)–N(1)	1.669(8)	S(2)–O(4)	1.450(6)
Fe(1)–N(2)	1.674(8)	S(2)–O(5)	1.466(6)
Fe(1)–S(1)	2.253(2)	S(2)–S(1)	2.136(3)
Fe(1)–S(1)$^{\#1}$	2.260(2)	S(3)–C(6)	1.664(9)
Fe(1)–Fe(1)$^{\#1}$	2.712(2)	O(1)–N(1)	1.183(10)
S(2)–O(3)	1.447(6)	O(2)–N(2)	1.150(10)
Angle	**ω, deg**	**Angle**	**ω, deg**
N(1)Fe(1)N(2)	118.9(4)	O(3)S(2)O(5)	115.0(4)
N(1)Fe(1)S(1)	107.8(3)	O(4)S(2)O(5)	111.9(4)
N(2)Fe(1)S(1)	108.6(3)	O(3)S(2)S(1)	102.0(3)
N(1)Fe(1)S(1)$^{\#1}$	108.9(3)	O(4)S(2)S(1)	104.3(3)
N(2)Fe(1)S(1)$^{\#1}$	105.8(3)	O(5)S(2)S(1)	107.5(3)
S(1)Fe(1)S(1)$^{\#1}$	106.12(8)	S(2)S(1)Fe(1)	108.50(11)
N(1)Fe(1)Fe(1)$^{\#1}$	121.6(3)	S(2)S(1)Fe(1)$^{\#1}$	107.82(11)
N(2)Fe(1)Fe(1)$^{\#1}$	119.4(3)	Fe(1)S(1)Fe(1)$^{\#1}$	73.87(8)
S(1)Fe(1)Fe(1)$^{\#1}$	53.18(7)	O(1)N(1)Fe(1)	169.5(7)
S(1)$^{\#1}$Fe(1)Fe(1)$^{\#1}$	52.94(7)	O(2)N(2)Fe(1)	172.5(8)
O(3)S(2)O(4)	114.6(4)		

* Symmetry codes used to generate equivalent atoms: $^{\#1}$ $-x + 1, -y + 1, -z + 1$.

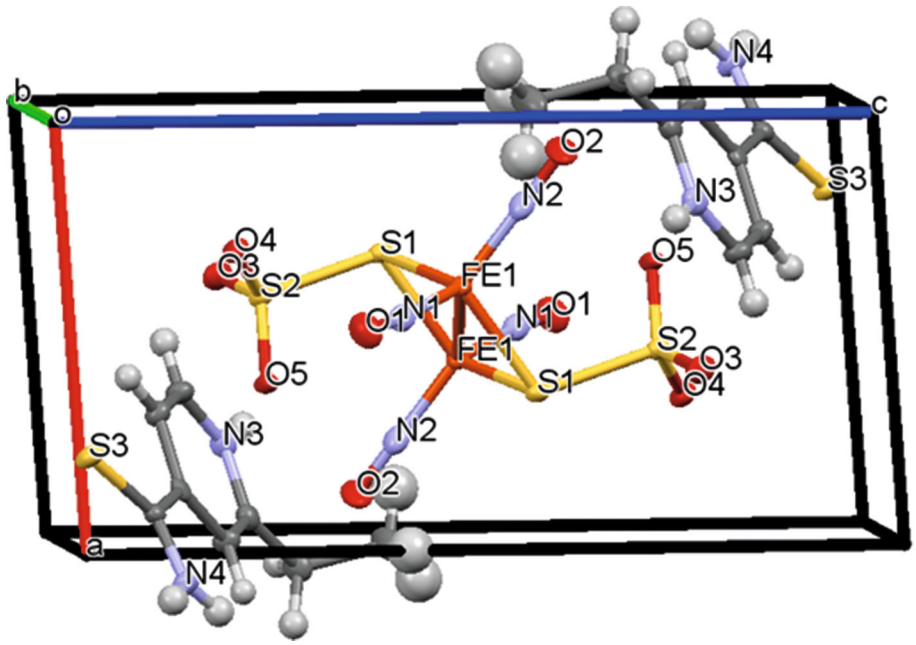

Fig. 2. Crystal packing of the structure of **I**.

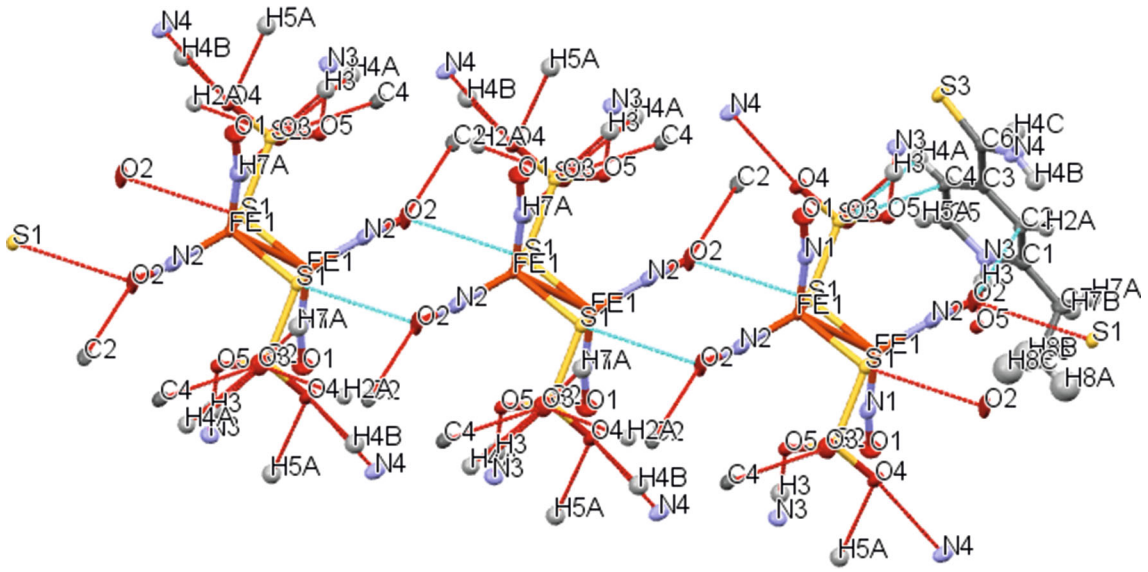

Fig. 3. Chains of the intermolecular contacts of the NO group of dianion **I**.

Thus, according to the data of amperometry, compound **I** more efficiently generates NO in aerobic aqueous solutions at physiological pH of 6.5–7.0, which makes it a promising NO donor for biomedical measurements.

The complex proved to be efficient against both gram-negative and gram-positive bacteria: its antibacterial action is comparable with the action of the kanamycin and streptomycin. Table 6 summarizes the MIC values for **I**, ethionamide, and a sodium salt with the $[Fe_2(S_2O_3)_2(NO)_4]^{2-}$ dianion. As can be seen from the obtained results, the components of complex **I**, that is, ethionamide and $[Fe_2(S_2O_3)_2(NO)_4]^{2-}$, do not show an antibacterial effect. The MIC values for them are more than 1000 μM. Thus, the antibacterial action of **I** is not determined by the action of its constituents.

Bacterial biofilms represent microbial communities surrounded by the matrix of extracellular polysaccharides produced by bacteria. The bacterial biofilms are more resistant to antibiotics than the planktonic forms, due to the presence of the protective barrier, which complicates the treatment of infections. Therefore, the search and development of alternative antibacterial compounds is highly relevant [66]. Figure 6 shows the influence of **I** and reference compounds in concentrations corresponding to MIC on the ability of *M. luteus* to form biofilms. Complex **I** efficiently inhibits the formation of *M. luteus* biofilms (39%), and its activity is comparable with or is markedly higher than that of the used antibiotics.

Table 3. Intermolecular contacts in complex **I**

Atom 1	Atom 2	*d*, Å
O(2)	S(1)	3.320
O(3)	C(4)	2.941
O(2)	C(2)	3.165

It is noteworthy that the antibacterial activity of **I** is twice as high as that of the thiobenzamide complex both in bacterial growth suppression experiments and in the studies of biofilm formation. The antibacterial efficiencies of INC **I** and the thiobenzamide complex are correlated with their NO-donor activity. Under the same experimental conditions, the thiobenzamide complex generates 5.0 nM of NO [52], while INC **I** produces 18.2 nM of NO. Meanwhile, analysis of a broad range of INCs indicates that there is no clear correlation between their antibacterial and NO-donor properties [52]. Perhaps, the antibacterial effect of INCs is due to the formation of long-lived nitrosyl intermediates.

The results of studying the cytotoxic action of **I** and ethionamide are depicted in Fig. 7. The IC_{50} values calculated from the curves are summarized in Table 6. As can be seen from Fig. 7, an increase in the concentration of **I** to 125 μM causes a decrease in the cell viability; further increase in the concentration of **I**, results in the viability being observed in 10% of the cell population. The structural components present in **I**, that is, ethionamide (Fig. 7, Table 7) and $Na_2[Fe_2(S_2O_3)_2(NO)_4]\cdot 4H_2O$ [52], possess low cytotoxic activity.

In the present work, the activity of **I** as a PDE inhibitor was also studied experimentally.

The PDE type hydrolytic enzymes cleave the phosphoester bond of cyclic nucleotides and thus reg-

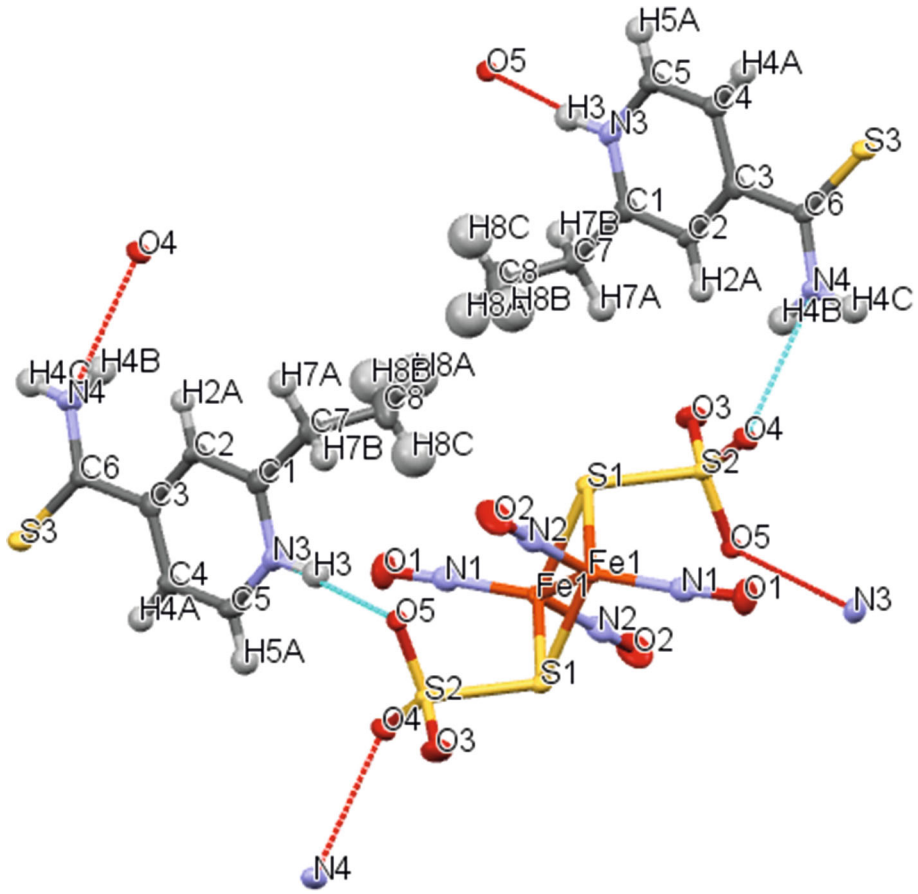

Fig. 4. Fragment of the crystal structure of **I**. The atoms are drawn as ellipsoids at 50% probability. The dashed lines show hydrogen bonds.

ulate their intracellular level [67]. The PDE inhibition results, in addition to guanylate cyclase activation by NO, in the accumulation of cyclic nucleotides acting as universal intracellular metabolism regulators [68]. It is known that phosphodiesterase inhibitors are widely used in medicine for the treatment of pulmonary arterial hypertension, chronic obstructive pulmonary disease, benign prostatic hyperplasia, erectile dysfunction, acute decompensated heart failure, psoriasis, atopic dermatitis, etc. [69–71].

The resulting data on the enzyme inhibition by **I** and ethionamide are given in Table 8. According to the obtained data, complex **I** present in the concentration range from 0.1 to 0.001 mM modulates the cGMP PDE activity. In the concentration of 0.1 mM, it inhibits the activity by 68.3%.

The action of **I** on the enzyme function was compared with the action of ethionamide, present as a constituent of **I**. It was shown that ethionamide in the used concentrations slightly inhibits the cGMP PDE;

Table 4. Geometric parameters of hydrogen bond in complex **I**

D–H...A	Distance, Å			DHA angle, deg	Coordinates of A atom
	D–H	H...A	D...A		
N(4)–H(4B)...O(4)	0.860	2.126	2.848	141.25	$x-1, y, z$
N(4)–H(4C)...S(3)	0.860	2.518	3.363	167.60	$-x, -y+1, -z+2$
N(3)–H(3)...S(2)	0.850	2.887	3.648	149.98	$x, y-1, z$
N(3)–H(3)...O(5)	0.850	1.829	2.672	170.85	$x, y-1, z$

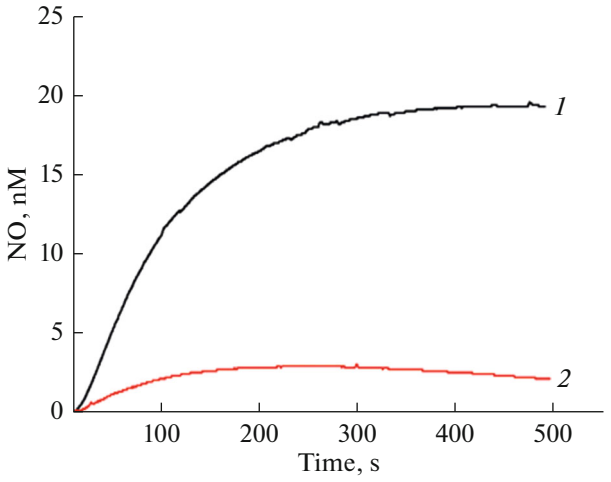

Fig. 5. Time dependences of the concentration of NO generated by **I** (0.4×10^{-5} M) in 0.1% aqueous solution of DMSO at pH 7.0 and $T = 25$°C under (*1*) aerobic and (*2*) anaerobic conditions.

in concentration of 0.1 mM, it inhibits the enzyme function 6.7 times less efficiently than complex **I**. Thus, the discovered ability of the test compound to inhibit the cGMP PDE enzyme may suggest a high therapeutic activity of this compound.

In order to gain a more comprehensive view on the mechanism of action of **I** on the enzyme, we used the kinetic method for investigation of enzymatic reactions, which provides data on the nature of enzyme binding to the inhibitor. The type of influence of the reversible inhibitor is determined by the dependence of the reciprocal enzymatic reaction rate ($1/V$) on the reciprocal substrate concentration ($1/S$) [61].

As can be seen from Fig. 8, complex **I** competitively inhibits cGMP PDE with the inhibition constant $K_i = 2.9 \times 10^{-4}$ M, which implies binding to the substrate active site.

Previously [60], the mechanism of action of $Na_2[Fe_2(S_2O_3)_2(NO)_4]\cdot 4H_2O$ on the enzymatic function of cGMP PDE was studied. It was shown that this complex inhibits the enzyme more efficiently than complex **I** does. In the concentrations of 0.1, 0.01, and 0.001 mM, the inhibition was 100, 87, and 65%, respectively. It was shown that it is a non-competitive inhibitor, i.e., it binds outside the enzyme active site with the inhibition constant $K_i = 1$ μM, which is two orders of magnitude lower than the constant for **I**. Apparently, in this case, a considerable role belongs to the counter-ion, protonated ethionamide, which, as follows Table 7, can itself inhibit PDE.

Thus, it was found by X-ray diffraction that ethionamide ($C_8H_{10}N_2S$) is protonated in highly acidic media at the pyridine nitrogen atom and replaces the Na^+ cation in $Na_2[Fe_2(S_2O_3)_2(NO)_4]\cdot 4H_2O$ to give the binuclear complex $(C_8H_{10}N_2S^+)_2[Fe_2(S_2O_3)_2(NO)_4]^{2-}$, which is an efficient NO donor under physiological conditions. It was shown that complex **I** has an antibacterial activity against both gram-negative and gram-positive microorganisms comparable to the activities of antibiotics kanamycin and streptomycin, and suppresses biofilm formation of *Micrococcus luteus* bacteria with an efficiency comparable to that of ceftriaxone. Data on the cytotoxic effects of complex **I** were obtained for the first time: the compound is toxic against the Vero cells with IC_{50} of about 70 μM. It was shown that complex **I** efficiently inhibits a hydrolytic enzyme, cyclic guanosine monophosphate phosphodiesterase, in the studied concentration range (0.1–0.01 mM); it competitively inhibits the enzyme function with the inhibition constant $K_i = 2.9 \times 10^{-4}$ M.

Table 5. Maximum amounts of NO generated by complex **I** (the concentration of the complex was 0.4×10^{-5} M) in 1% aqueous solutions of DMSO at different pH

pH	NO, nM	
	anaerobic conditions	aerobic conditions
6.5	11.2	19.3
7.0	2.8	18.2
8.0	2.8	0.4
9.0	9.1	1.0

Table 6. MIC values for the test compounds

Compound	MIC, μM	
	M. luteus	*E. coli*
I	31.25	62.5
Ethionamide	>1000	>1000
$Na_2[Fe_2(S_2O_3)_2(NO)_4]\cdot 4H_2O$	>1000	>1000
Ampicillin	0.98	3.9
Kanamycin	62.5	31.25
Streptomycin	125	62.5
Ceftriaxone	3.9	0.98

FUNDING

This study was supported by the Ministry of Science and Higher Education of the Russian Federation (State Assignment no. AAAA-A19-119071890015-6).

Table 7. IC_{50} values of test compounds against Vero cells

Compound	IC_{50}, μM
I	69.27 ± 3.45
Ethionamide	>500
$Na_2[Fe_2(S_2O_3)_2(NO)_4]\cdot 4H_2O$	>500

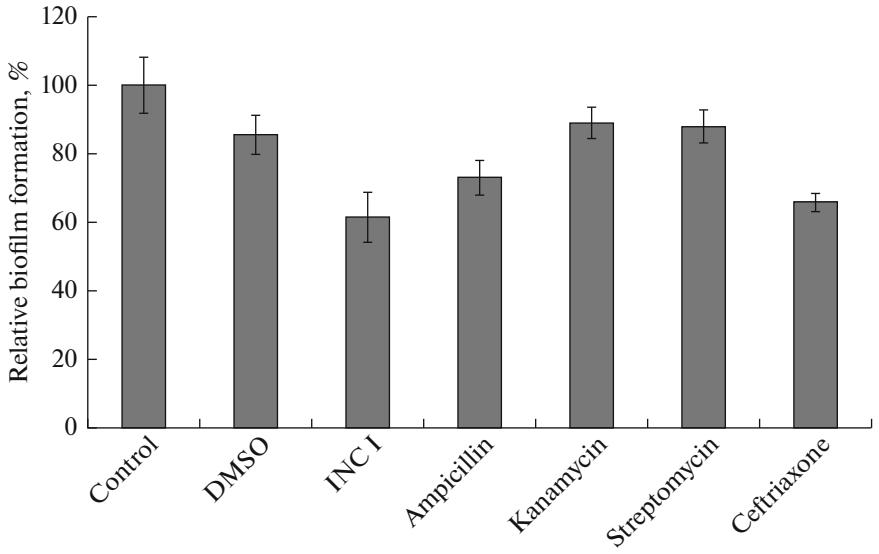

Fig. 6. Efficiency of formation of the *M. luteus* biofilm on exposure to the test compounds in the MIC dose 24 h after the introduction.

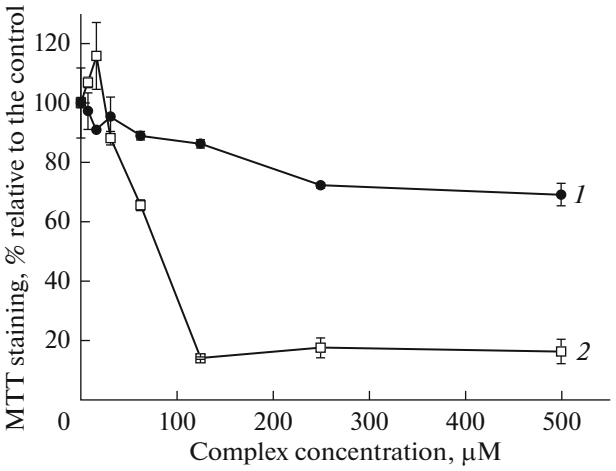

Fig. 7. Dose–effect curves for Vero cells 72 h after treatment with (*1*) ethionamide and (*2*) complex **I**.

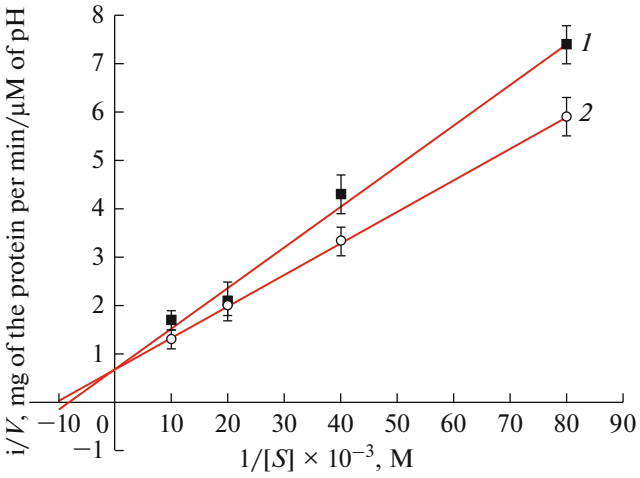

Fig. 8. Reciprocal rate of cGMP hydrolysis vs. reciprocal substrate concentration (0.1, 0.05, 0.025, and 0.0125 mM) in the Lineweaver–Burk coordinates: (*1*) in the presence of 1×10^{-4} M of **I** and (*2*) in the absence of the complex.

Table 8. Inhibition of cGMP PDE (% of the control) by **I** and ethionamide

Compound	Inhibition of enzyme activity (% of the control)		
	concentration, mM		
	0.1	0.01	0.001
I	68.3	17.1	14.3
Ethionamide	10.3	5.1	2.6

CONFLICT OF INTEREST

The authors of this work declare that they have no conflicts of interest.

REFERENCES

1. Benencia, F. and Courreges, M.C., *Immunology*, 1999, vol. 98, no. 3, p. 363.
2. Mehta, D.R., Ashkar, A.A., and Mossman, K.L., *PLoS One*, 2012, vol. 7, no. 2, p. e31688.
3. McMullin, B.B., Chittock, D.R., Roscoe, D.L., et al., *Respiratory Care*, 2005, vol. 50, no. 11, p. 1451.
4. Jones-Carson, J., Zweifel, A.E., Tapscott, T., et al., *PLoS Negl. Trop. Dis.*, 2014, vol. 8, no. 8, p. e3079.
5. Fang, F.C., *J. Clin. Invest.*, 1997, vol. 99, no. 12, p. 2818.
6. De Groote, M.A. and Fang, F.C., *Clin. Infect. Dis.*, 1995, vol. 21, no. 2, p. S162.
7. Schairer, D.O., Chouake, J.S., Nosanchuk, J.D., et al., *Virulence*, 2012, vol. 3, p. 271.
8. Jones, M.L., Ganopolsky, J.G., Labbe, A., et al., *Appl. Microbiol. Biotechnol.*, 2010, vol. 88, no. 2, p. 401.
9. Jones, M.L., Ganopolsky, J.G., Labbe, A., et al., *Appl. Microbiol. Biotechnol.*, 2010, vol. 87, no. 2, p. 509.
10. Fox, S., Wilkinson, T.S., Wheatley, P.S., et al., *Acta Biomater.*, 2010, vol. 6, no. 4, p. 1515.
11. Narin, G., Albayrak, C.B., and Ulku, S., *Appl. Clay Sci.*, 2010, vol. 50, no. 4, p. 560.
12. Weller, R., Ormerod, A.D., Hobson, R.P., et al., *J. Am. Acad. Dermatol.*, 1998, vol. 38, no. 4, p. 559.
13. Ormerod, A.D., White, M.I., Shah, S.A., et al., *Br. J. Dermatol.*, 1999, vol. 41, no. 6, p. 1051.
14. Phillips, R., Adjei, O., Lucas, S., et al., *Antimicrob. Agents Chemother.*, 2004, vol. 48, no. 8, p. 2866.
15. Ormerod, A.D., Shah, A.A., Li, H., et al., *BMC Res. Notes*, 2011, vol. 4, p. 458.
16. Davidson, R.N., Yardley, V., Croft, S.L., et al., *Trans. R. Soc. Trop. Med. Hyg.*, 2000, vol. 94, no. 3, p. 319.
17. Daiber, A., Wenzel, P., Oelze, M., et al., *Clin. Res. Cardiol.*, 2008, vol. 97, no. 1, p. 12.
18. Deupree, S.M. and Schoenfisch, M.H., *Acta Biomater.*, 2009, vol. 5, no. 5, p. 1405.
19. Schairer, D.O., Chouake, J.S., Nosanchuk, J.D., and Friedman, A.J., *Virulence*, 2012, vol. 3, no. 3, p. 271.
20. Cariello, A.J. and Bispo, P.J., de Souza, et al., *Clin. Ophthalmol.*, 2012, vol. 6, p. 1907.
21. Williams, D.L.H., *Acc. Chem. Res.*, 1999, vol. 32, no. 10, p. 869.
22. Laver, J.R., Stevanin, T.M., Messenger, S.L., et al., *FASEB J.*, 2010, vol. 24, no. 1, p. 286.
23. Jaouen, G. and Salmain, M., *The Bioorganometalic Chemistry: Applications in Drug Discovery, Biocatalysis and Imaging*, Weinheim: Wiley-VCH, 2014.
24. Hsiao, H., Chung, C., Santos, J.H., et al., *Dalton Trans.*, 2019, vol. 48, p. 9431.
25. Gould, N., Doulias, P.-T., Tenopoulou, M., et al., *J. Biol. Chem.*, 2013, vol. 288, no. 37, p. 26473.
26. Stupina, T.S., Antonova, N.O., Balalaeva, I.V., et al., *Intern. Sci. J. Med. Biol. Sci.*, 2014, vol. 1, no. 1, p. 23.
27. Grigor'ev, A.I. and Vladimirov, Yu.A., *Fundamental'nye nauki — meditsine: Biofizicheskie meditsinskie tekhnologii* (Fundamental Sciences for Medicine: Biophysical Medical Technologies), Moscow: MAKS Press, 2015.
28. Sanina, N.A., Kozub, G.I., Kondrat'eva, T.A., et al., *Russ. Chem. Bull.*, 2017, no. 9, p. 1706.
29. Mumyatova, V.A., Kozub, G.I., Kondrat'eva, T.A., et al., *Russ. Chem. Bull.*, 2019, no. 5, p. 1025.
30. Sanina, N.A., Mumyatova, V.A., Terent'ev, A.A., et al., *Russ. Chem. Bull.*, 2019, no. 12, p. 2225.
31. Hanoulle, X., Wieruszeski, J.M., Rouseelot-Pailley, P., et al., *Biochem. Biophys. Res. Commun.*, 2005, vol. 331, p. 452.
32. Vilchèze, C., Weisbrod, T.R., Chen, B., et al., *Antimicrob. Agents Chemother.*, 2005, vol. 49, p. 708.
33. Yu, K.L., Torri, A.F., Luo, G., et al., *Bioorg. Med. Chem. Lett.*, 2002, vol. 12, no. 23, p. 3379.
34. Hitotsuyanagi, Y., Hasuda, T., Matsumoto, Y., et al., *Chem. Commun.*, 2000, no. 17, p. 1633.
35. Nakagawa, Y., Irie, K., Ohigashi, H., et al., *Bioorg. Med. Chem. Lett.*, 2000, vol. 10, no. 18, p. 2087.
36. Wei, Q.L., Zhang, S.S., Gao, J., et al., *Bioorg. Med. Chem.*, 2006, vol. 14, no. 21, p. 7146.
37. Wentland, M.P., Sun, X., Bu, Y., et al., *Bioorg. Med. Chem. Lett.*, 2005, vol. 15, no. 10, p. 2547.
38. Krinková, J., Doležal, M., Hartl, J., et al., *Il Farmaco*, 2002, vol. 57, no. 1, p. 71.
39. Yu, K.L., Torri, A.F., Luo, G., et al., *Bioorg. Med. Chem. Lett.*, 2002, vol. 12, no. 23, p. 3379.
40. Davies, D.J., Faust, R., Garratt, P.J., et al., *Bioorg. Chem.*, 2004, vol. 32, no. 1, p. 1.
41. Boström, J., Olsson, R.I., Tholander, J., et al., *Bioorg. Med. Chem. Lett.*, 2010, vol. 20, no. 2, p. 479.
42. Thanigaimalai, P., Sharma, V.K., Lee, K.C., et al., *Bioorg. Med. Chem. Lett.*, 2010, vol. 20, no. 16, p. 4771.
43. Brunhofer, G., Studenik, C., Ecker, G.F., et al., *Eur. J. Pharm. Sci.*, 2011, vol. 42, nos. 1–2, p. 37.
44. Shimotori, Y., Hoshi, M., Ogawa, N., et al., *Heterocycl. Commun.*, 2020, vol. 26, p. 84.
45. *Registr lekarstvennykh sredstv Rossii: Entsiklopediya lekarstv. Vyp. 29* (Register of Pharmaceutical Products of Russia: Drug Encyclopedia. Issue 29), Vyshkovskii, G.L., Ed., Moscow: Vedanta, 2021.
46. Mahantaa, N., Szantai-Kisc, M., Peterssonc, E.J., et al., *ACS Chem. Biol.*, 2019, vol. 14, no. 2, p. 142.
47. Vale, N., Gomes, P., and Santos, H., *Curr. Drug Metab.*, 2013, vol. 14, no. 1, p. 151.
48. Mills III, T. and Roberson, J.C., *Instrumental Data for Drug Analysis*, New York: Elsevier, 1992, vol. 2.
49. Eccles, K.S., Morrison, R.E., Maguire, A.R., et al., *Cryst. Growth Des.*, 2014, vol. 14, p. 2753.
50. Wysokinski, R., Michalska, D., Bienko, D.C., et al., *J. Mol. Struct.*, 2006, vol. 791, nos. 1–3, p. 70.
51. Vale, N., Makila, E., Salonen, J., et al., *Eur. J. Pharm. Biopharm.*, 2012, vol. 81, p. 314.
52. Sanina, N.A., Starostina, A.A., Utenyshev, A.N., et al., *Molecules*, 2022, vol. 27, p. 6886.

53. Karyakin, Yu.V. and Angelov, I.I., *Chistye khimicheskie veshchestva* (Pure Chemicals), Moscow: Khimiya, 1974.

54. Sanina, N.A., Aldoshin, S.M., and Rudneva, T.N., *Russ. J. Coord. Chem*., 2005, vol. 31, no. 5, p. 301. https://doi.org/10.1007/s11173-005-0093-3

55. Weissberger, A., Proskauer, E., Riddick, J.A., et al., *Organic Solvents: Physical Properties and Methods of Purification*, New York: Intercscience, 1955.

56. *Agilent. CrysAlis PRO*, Yarnton–Oxfordshire: Agilent Technologies UK Ltd., 2011.

57. Sheldrick, G.M., *SHELXTL. Version 6.14. Structure Determination Software Suite*, Madison (WI, USA): Bruker AXS, 2000.

58. *MUK 4.2.1890-04. Opredelenie chuvstvitel'nosti mikroorganizmov k antibakterial'nym preparatam. Metodicheskie ukazaniya: data vvedeniya 2014-03-04* (MUK 4.2.1890-04. Determination of Bacterial Sensitivity to Antiibacterial Agents. Methodical Guidelines: Issued April 3, 2014) Moscow: Federal'nyi tsentr gossanepidnadzora Minzdrava Rossii, 2004.

59. Libinzon, R.E., Shchekoldina, T.G., Batolkina, O.E., et al., *Voprosy meditsinskoi khimii*, 1977, vol. 23, no. 4, p. 526.

60. Tat'yanenko, L.V., Kotel'nikov, A.I., Dobrokhotova, O.V., et al., *Khim.-Farm. Zh*., 2009, vol. 43, no. 9, p. 45.

61. Berezin, I.V. and Klesov, A.A., *Prakticheskii kurs khimicheskoi i fermentativnoi kinetiki* (Practical Course of Chemical and Enzymatic Kinetics), Moscow: Izd-vo Mosk. un-ta, 1976.

62. Glidewell, C., Hursthouse, M.B., Lambert, R.J., et al., *Dalton Trans*., 1989, p. 2061.

63. Sanina, N.A., Rakova, O.A., Aldoshin, S.M., et al., *Russ. J. Coord. Chem*., 2001, vol. 27, no. 3, p. 179. https://doi.org/10.1023/A:1009598228585

64. Sanina, N.A., Emel'yanova, N.S., Chekhlov, A.N., et al., *Russ. Chem. Bull.*, 2010, vol. 59, p. 1126.

65. Sanina, N.A., Sulimenkov, I.V., Rudneva, T.N., et al., *Dokl. Chem.*, 2009, vol. 425, Pt. 1, p. 60.

66. Chan, C., Hardin, T.C., and Smart, J.I., *Future Microbiol.*, 2015, vol. 10, p. 1325.

67. Omori, K. and Kotera, J., *Circ. Res.*, 2007, vol. 100, p. 309.

68. Hardman, J.G., Robison, G.A., and Sutherland, E.W., *Annu. Rev. Physiol.*, 1971, vol. 33, p. 311.

69. Padda, I.S. and Tripp, J., *Phosphodiesterase Inhibitors*, Treasure Island (FL): StatPearls, 2022.

70. Baillie, G.S., Tejeda, G.S., and Kelly, M.P., *Nat. Rev. Drug Discov*., 2019, vol. 18, p. 770.

71. Miller, M.S., *J. Receptor Ligand Channel Res*., 2015, vol. 8, p. 19.

Translated by Z. Svitanko